

AVM-SLAM: Semantic Visual SLAM with Multi-Sensor Fusion in a Bird’s Eye View for Automated Valet Parking

Ye Li^{1,2,3}, Wenchao Yang³, Ju Tao³, Qianlei Wang^{1,2}, Zhe Cui^{1,2}, and Xiaolin Qin^{1,2}

Abstract—Automated Valet Parking (AVP) requires precise localization in challenging garage conditions, including poor lighting, sparse textures, repetitive structures, dynamic scenes, and the absence of Global Positioning System (GPS) signals, which often pose problems for conventional localization methods. To address these adversities, we present AVM-SLAM, a semantic visual SLAM framework with multi-sensor fusion in a Bird’s Eye View (BEV). Our framework integrates four fisheye cameras, four wheel encoders, and an Inertial Measurement Unit (IMU). The fisheye cameras form an Around View Monitor (AVM) subsystem, generating BEV images. Convolutional Neural Networks (CNNs) extract semantic features from these images, aiding in mapping and localization tasks. These semantic features provide long-term stability and perspective invariance, effectively mitigating environmental challenges. Additionally, data fusion from wheel encoders and IMU enhances system robustness by improving motion estimation and reducing drift. To validate AVM-SLAM’s efficacy and robustness, we provide a large-scale, high-resolution underground garage dataset, available at <https://github.com/yale-cv/avm-slam>. This dataset enables researchers to further explore and assess AVM-SLAM in similar environments.

I. INTRODUCTION

Automated Valet Parking (AVP) has recently gained momentum as a solution to alleviate parking congestion and improve driver convenience. It is typically employed in semi-enclosed spaces with low speeds and no passengers, making it well-suited for achieving Level 4 autonomous driving. In this context, the primary technical challenge is achieving precise mapping and localization. However, parking garages often present challenges, such as poor lighting, limited texture diversity, repetitive architectural layouts, changing environmental conditions, and the absence of Global Positioning System (GPS) signals. These factors pose substantial obstacles for traditional localization methods.

To tackle this challenge, we employ semantic attributes derived from garage road markings to build the map and localize the vehicle, as shown in Fig. 1. These semantic characteristics offer enduring stability and perspective invariance, including lane lines, parking spots, zebra crossings, and indicating arrows. Extracting these semantic features is accomplished using Convolutional Neural Networks (CNNs) working on Bird’s Eye View (BEV) image. The BEV image is captured by surrounding cameras and generated by the Around View Monitor (AVM) subsystem.

¹Chengdu Institute of Computer Applications, Chinese Academy of Sciences, Chengdu, Sichuan 610041, China. yale.li.cn@gmail.com, cui zhe@casit.com.cn, qinxl2001@126.com

²University of Chinese Academy of Sciences, Beijing 100049, China

³Jiayu Intelligent Technology Co.,Ltd. (Affiliated With Great Wall Motor Company Limited), Shanghai 200335, China

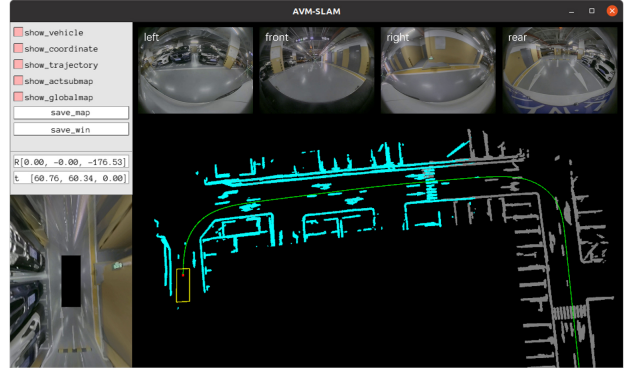


Fig. 1: Semantic visual map of the garage build by our AVM-SLAM system. It fuses data from surround view cameras, wheel encoder and IMU in a bird’s eye view.

In certain extreme scenarios, the extraction of semantic features might encounter difficulties. As technology has progressed, wheel encoders and IMUs have become more affordable and nearly standard equipment in vehicle sensor arrays. Consequently, a multi-sensor hybrid fusion approach has been devised, distinct from both loosely and tightly methods, to amalgamate data from various sensors, resulting in the development of the AVM-SLAM system, which stands for “a semantic visual SLAM with multi-sensor fusion in a bird’s-eye view perspective.”

Furthermore, a large-scale and high-resolution dataset has been created and published, comprising synchronized multi-sensor data collected within an underground garage. This dataset serves to validate the effectiveness and robustness of the aforementioned methods. In summary, the primary contributions of this article can be outlined as follows:

- A pragmatic and innovative semantic visual SLAM framework, known as AVM-SLAM, has been developed. It integrates multiple sensors and employs a bird’s-eye view perspective, enabling robust and efficient operation within underground garages.
- A multi-sensor hybrid fusion strategy has been developed to enhance robustness and efficiency, distinct from both loosely and tightly approaches. This strategy aims to maximize the benefits of multi-sensor fusion.
- A large-scale and high-resolution dataset of typical underground garage data, contains four surround cameras’ images, one synthesized bird’s eye view, four wheel encoders’ measurements and an IMU’s measurements. This dataset will be beneficial for further research in SLAM, especially for autonomous vehicle localization in underground garages.

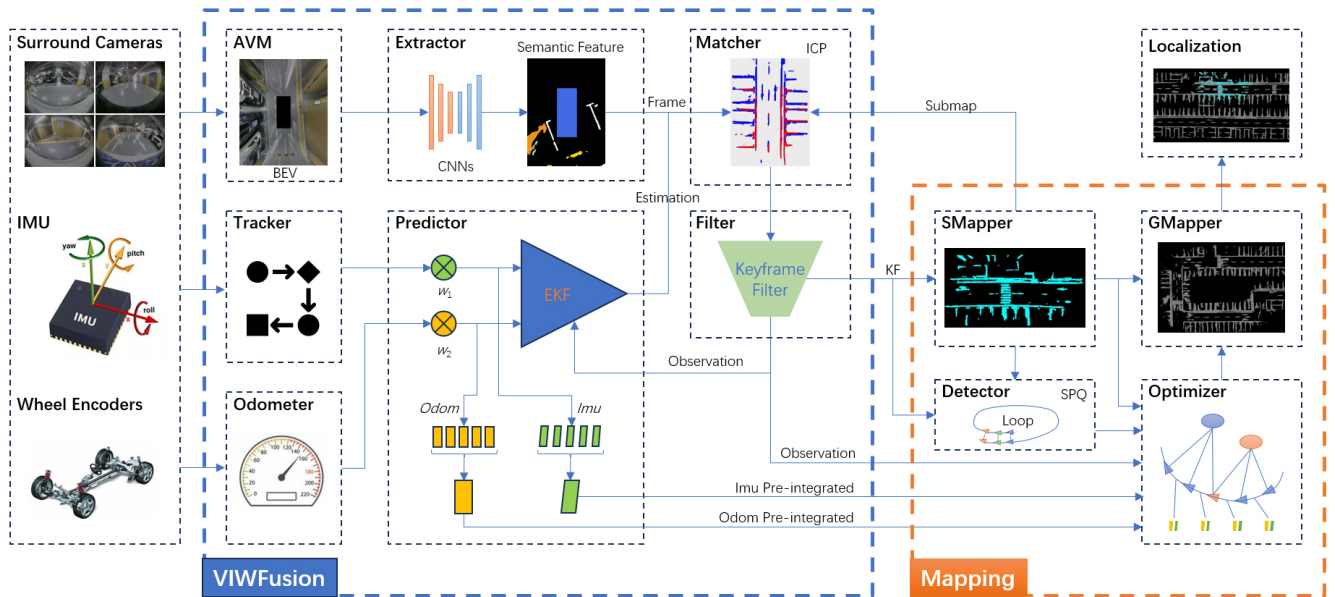


Fig. 2: The framework of the proposed AVMSLAM system consists of two core modules: VIWFusion and Mapping. VIWFusion is a loosely multi-sensor weighted fusion front-end, while the Mapping module serves as a tightly integrated semantic mapping back-end. w_1 and w_2 are the fusion weights for IMU and wheel odometry, respectively.

II. RELATED WORK

A. Traditional Visual SLAM and Lidar SLAM

Over the past decade, traditional SLAM fields have witnessed the emergence of numerous exceptional solutions. These solutions typically employ conventional texture and 3D structural features of the environment for mapping and localization purposes. Examples include ORB-SLAM [1]–[3], which relies on the ORB visual feature, SVO [4], and DSO [5], both leveraging optical flow. Additionally, Cartographer [6], LOAM [7], and LeGO-LOAM [8] are based on 2D/3D lidar structural features. These approaches have demonstrated impressive performance in scenarios characterized by ample lighting, rich textures, and well-defined structures.

B. Methods of Multi-Sensor Fusion

Both lidar and visual sensors have inherent limitations. Lidar is sensitive to structural information and can fail in structure-scarce environments. Visual sensors are sensitive to texture and can fail in scenarios with poor textures, low lighting, or overexposure.

In recent years, SLAM technology has shifted towards multi-sensor fusion, progressing from visual-inertial fusion to lidar-inertial fusion and ultimately fusing lidar, visual, inertial sensors, wheel encoders, and GPS data. Notable advancements include VINS-Mono [9], VINS-Fusion [10], and OpenVINS [11] for visual-inertial fusion, LIC-Fusion [12] and VIL-SLAM [13] for lidar-visual-inertial fusion, [14] and [15] for enhanced fusion with wheel encoders, VIWO [16] for sliding-window filtering to fuse multi-modal data, and [17] for introducing wheel encoder pre-integration theory and noise propagation formula, enabling tight integration with sensor data.

By amalgamating data from multiple sensors, these approaches significantly enhance simultaneous localization and mapping robustness and accuracy.

C. Semantic Visual SLAM for AVP

Semantics-enhanced visual SLAM is crucial for autonomous driving, particularly AVP applications. Challenges in garage environments persist for both visual and lidar SLAM, driving the need for enduring semantic features.

Research by H. Grimmer [18] and U. Schwesinger [19] explores mapping and localization using surround cameras and semantic features. Z. Xiang [20] extracts free space contours for pose tracking from a bird’s-eye view, creating virtual lidar points. J. Hu [21] and T. Qin [22] develop a comprehensive visual SLAM system using road markings for mapping and parking facility localization. X. Shao [23] establishes tightly-coupled semantic SLAM with visual, inertial, and surround-view sensors. Z. Xiang [24] utilizes hybrid edge information from bird’s-eye view images to enhance semantic SLAM, while C. Zhang [25] leverages HD vector map directories for parking lot localization. These studies offer valuable insights for future research.

III. FRAMEWORK

This paper introduces the AVMSLAM system, consisting of two core modules: VIWFusion and Mapping, as shown in Fig. 2. Our design utilizes a unique multi-sensor hybrid fusion strategy, departing from traditional approaches, ensuring seamless collaboration between these modules for maximum multi-sensor fusion benefits.

VIWFusion is a loosely-coupled, multi-sensor weighted fusion front-end, encompassing the AVM subsystem, Semantic Extractor and Matcher, IMU Tracker, Wheel Odometer, Pose Predictor, and Keyframe Filter. It applies weighted

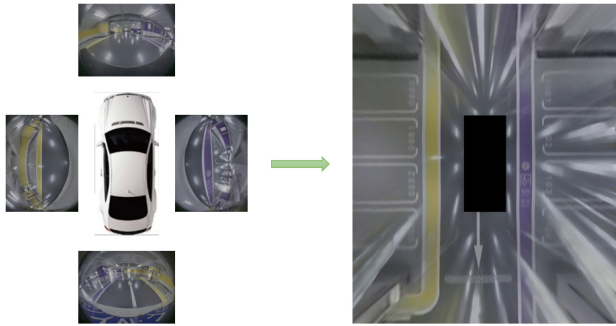


Fig. 3: Generate bird’s eye view from surround fisheye images by AVM

fusion to data from surround cameras, wheel encoders, and IMU sensors, rooted in Extended Kalman Filter (EKF) theory, providing initial values for visual semantic matching and kinematic constraints for subsequent back-end optimization through pre-integrated (IMU and wheel) values among adjacent semantic keyframes.

The Mapping module is a tightly-coupled, semantic mapping back-end, comprising the Loop Detector, Global Optimizer, Sub Mapper, and Global Mapper. We utilize semantic ICP registration for loop detection, incorporating a semantic pre-qualification (SPQ) mechanism to streamline loop detection and minimize mismatches. Extra multi-sensor kinematic constraints, like pre-integrated values of IMU and Wheel between adjacent keyframes, expedite global optimization convergence and enhance mapping accuracy.

IV. METHOD

A. Around View Monitor

The AVM is crucial for generating BEV images and enhancing the SLAM system’s perceptual range and robustness. It undistorts and applies Inverse Perspective Mapping (IPM) to fisheye images from the four surrounding cameras, merging them into a comprehensive BEV image (see Fig. 3). The four surrounding cameras are strategically positioned around the vehicle, with offline calibrated intrinsic and extrinsic parameters. The virtual BEV camera is precisely located above the vehicle’s center, with its optical axis aligned vertically downward. Relevant intrinsic and extrinsic parameters for this virtual camera are derived through the IPM process.

In this section, we use the widely accepted generic fisheye camera model proposed by Kannala and Brandt [26] to rectify distortion, applying the following equation:

$$r(\theta) = k_1\theta + k_2\theta^3 + k_3\theta^5 + k_4\theta^7 + k_5\theta^9 \quad (1)$$

where θ is the angle between the principal axis and the incoming ray, r is the distance between the image point and the principal point, $k_i (i = 0, 1, 2, 3, 4)$ is the coefficient of distortion correction, calculated by offline calibration.

The IPM projection can be formulated as the follows:

$$\begin{bmatrix} u_{bev} \\ v_{bev} \\ 1 \end{bmatrix} = H * \begin{bmatrix} u_{undist} \\ v_{undist} \\ 1 \end{bmatrix} \quad (2)$$

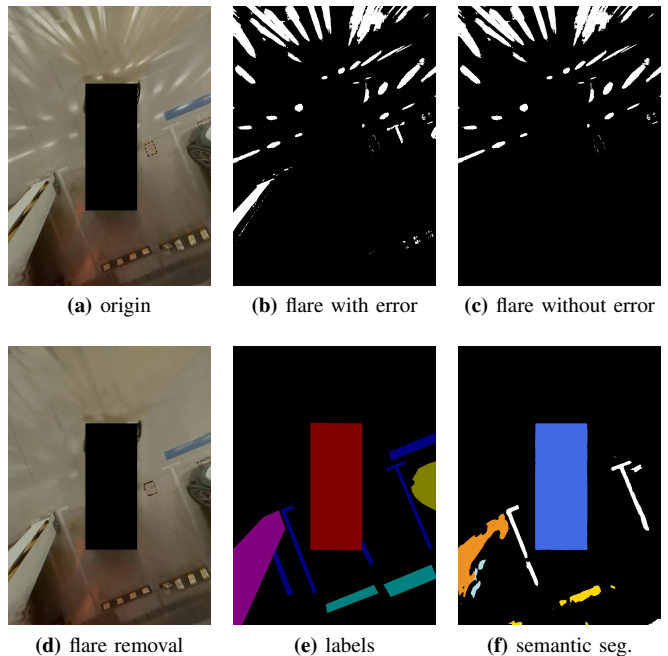


Fig. 4: Flare removal and semantic segmentation

where $[u_{undist} \ v_{undist}]$ is the pixel location in the undistortion fisheye image. $[u_{bev} \ v_{bev}]$ is the pixel location in the bird’s eye view. H is the homography matrix from undistortion fisheye image to bird’s eye view.

B. Semantic Extractor and Matcher

• Flare Removal

The ground’s light reflection creates diverging flares in the bird’s eye view, interfering with road marking line extraction (Fig. 4a). To address this issue, we propose a flare removal model based on the U-Net architecture [27], incorporating perceptual [28] and L1 losses for improved performance.

We efficiently generate flare-removed data for model training by using a specular highlight detection algorithm [29] to create a highlight mask (Fig. 4b). This mask is then refined by merging it with manually annotated foreground information to eliminate false detections (Fig. 4c). Finally, we apply an image inpainting algorithm [30] to effectively remove highlights (Fig. 4d).

This approach simplifies the labor-intensive process of labeling flare removal data.

• Semantic Extractor

The garage’s road markings, including lane lines, parking spots, zebra crossings, and indicating arrows, exhibit enduring stability and remain perspective-invariant. These qualities make them ideal for semantic visual mapping and vehicle localization.

We conducted a comparative analysis of semantic segmentation networks [31]–[34] and ultimately selected DDRnet [34], which balances efficiency and accuracy, for extracting road markings from the BEV images. Fig. 4e illustrates the semantic labels, and Fig. 4f showcases the segmentation results.

After segmentation, the results are downsampled for efficiency and then reconstructed into 3D space in the virtual BEV camera coordinate system, as shown below:

$$\begin{bmatrix} x_c \\ y_c \\ z_c \end{bmatrix} = K^{-1} * \begin{bmatrix} u_{bev} \\ v_{bev} \\ 1 \end{bmatrix} \quad (3)$$

where K is the intrinsic parameter of the virtual BEV camera. K^{-1} is the inverse of the K . $[x_c \ y_c \ z_c]$ is the 3D coordinate value in the virtual BEV camera coordinate system, in this case, the z_c of the semantic features on the ground are always equal to 1 meter.

Finally, transfer the 3D semantic features from virtual BEV camera coordinate into vehicle coordinate as follows:

$$\begin{bmatrix} x_v \\ y_v \\ z_v \\ 1 \end{bmatrix} = T_{vc} * \begin{bmatrix} x_c \\ y_c \\ z_c \\ 1 \end{bmatrix} \quad (4)$$

where $[x_v \ y_v \ z_v]$ is the 3D coordinate value in the vehicle coordinate system. T_{vc} is the transformation matrix from virtual BEV camera coordinate system to vehicle coordinate system, which calibrated offline.

- Semantic Matcher

In this task, we employ the Iterative Closest Point (ICP) algorithm for matching 3D semantic features. The cumulative error issue inherent in frame-to-frame matching is mitigated by implementing frame-to-map matching. This approach offers efficiency and robustness, particularly when equipped with a reliable initial pose estimation. The initial pose estimation is facilitated by a pose predictor that integrates data from an IMU and a wheel encoder.

C. Pose Predictor

- System Initialization

The proposed AVM-SLAM system is centered around BEV semantic features. Therefore, the pose predictor always considers the time t_0 of the first frame in the BEV semantic frame data queue *deqBevCam* as the initial candidate time for initialization. To determine if system initialization is possible, we assess the fusion mode settings and check whether there is data in the selected sensors' data queues before time t_0 . System initialization occurs only when data is available at time t_0 and earlier in all selected sensors' data queues. If these conditions aren't met, we remove the first frame from *deqBevCam* and continue evaluating the time t_1 of the next semantic frame. The system initializes successfully when the specified conditions are met. At this point, the vehicle coordinate system serves as both the initial coordinate system for the global map and the initial coordinate system for the first submap.

To enhance initialization accuracy, we perform linear interpolation on the data in the selected sensors' data queues to obtain data corresponding to the time of the relevant semantic frame.

- Pose Prediction

There is evidence that the linear velocity accuracy of the wheel odometry is higher when the vehicle is doing linear motion, and the angular velocity accuracy of the IMU is higher when it is doing rotational motion, and the two are obviously complementary. In order to improve the accuracy and robustness of the pose prediction, this paper adopts the EKF approach to weighted fusion multiple sensors' data. The fusion process is divided into a prediction step and an update step.

The prediction step can be described by the prediction equations 5 and 6, as shown below:

$$\hat{x}_k = f(\hat{x}_{k-1}, u_{k-1}) \quad (5)$$

$$P_k = F_k P_{k-1} F_k^T + Q_k \quad (6)$$

where \hat{x}_k is estimated state vector at time k . f is non-linear state transition function. u_{k-1} is control input at time $k-1$. P_k is covariance matrix of the state estimation error at time k . F_k is Jacobian matrix of the state transition function with respect to the state variables. Q_k is process noise covariance matrix at time k .

The update step can be described by the update equations 7-9, as the follows:

$$K' = P_k H_k^T (H_k P_k H_k^T + R_k)^{-1} \quad (7)$$

$$\hat{x}'_k = \hat{x}_k + K' (\vec{z}_k - h(\hat{x}_k)) \quad (8)$$

$$P'_k = (I - K' H_k) P_k \quad (9)$$

where K' is Kalman gain matrix at time k . H_k is measurement Jacobian matrix at time k . R_k is measurement noise covariance matrix at time k . \vec{z}_k is measurement vector at time k . h is non-linear measurement function. I is identity matrix.

Along with the multi-sensor weighted fusion pose prediction, we also pre-integrated the IMU and wheel odometry data between two consecutive keyframes for further optimization of the global pose-graph.

D. SubMapper and GlobalMapper

To enhance the efficiency of semantic feature ICP matching between frames and the map, we employ a keyframe-submap-globalmap structure for constructing the semantic map (Fig. 5). Semantic frames are filtered by the KeyFrame-Filter and inserted into the submap if they exhibit more than 50% difference with the previous keyframe. Each submap contains a fixed number of keyframes, typically 10 frames, but this can be adjusted as needed. The number of semantic points in the submap is significantly lower than in the global map, improving efficiency during frame-to-submap semantic feature ICP matching and reducing error accumulation in frame-to-frame matching.

Within the Mapping module, we maintain two submaps: the current submap and the upcoming submap, ensuring sufficient co-visibility area between adjacent submaps (set at 50% in this system). Keyframes are simultaneously inserted into both submaps. Once the maximum number of keyframes is reached in the current submap, we execute point cloud correction and local optimization. Then, the current submap

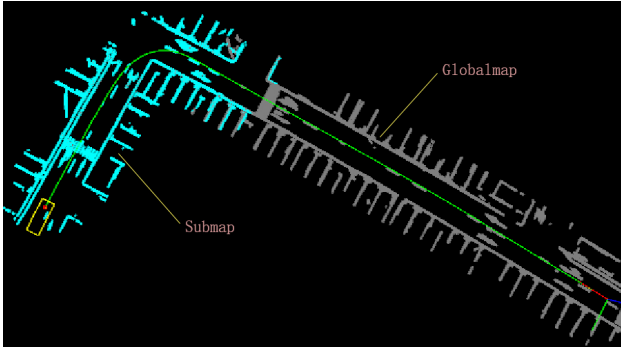


Fig. 5: Cyan submap and gray global map. The global map consists of submaps, which consist of keyframes.

is integrated into the global map, and the next submap takes its place, starting the creation of a new subsequent submap.

E. Loop Detector

Loop detection is crucial for global optimization, affecting mapping scale and SLAM speed. In complex environments, like underground garages with repetitive structures, not all keyframes and submaps are suitable for loop detection. To address this, we’ve developed SPQ (Semantic Pre-qualification) mechanism to filter potential loop frames and submaps, reducing detection and preventing mismatches.

SPQ evaluates candidates based on the category number and weights of semantic features within keyframes and submaps. Candidates exceeding a preset threshold qualify as loop frames and submaps. And then, added to the loop sequences for subsequent ICP semantic matching.

F. Global Optimizer

We employ a pose-graph approach for global optimization. As depicted in Fig. 6, the pose-graph’s Nodes encompass both keyframes and submaps, while Edges represent constraints involving keyframe-to-keyframe and keyframe-to-submap. Keyframe-to-keyframe constraints encompass semantic visual constraints between adjacent keyframes, alongside additional kinematic constraints derived from pre-integrated values (IMU and Wheel). Keyframe-to-submap constraints involve semantic visual constraints between keyframes and submaps, along with semantic loop constraints obtained from semantic loop detection. The global optimizer periodically performs optimization operations on the collected Nodes and Edges, subsequently updating the results for each keyframe and submap.

V. EXPERIMENTS

A. Benchmark Dataset

To validate the proposed AVM-SLAM system, tests were conducted in a 220m×110m underground garage with over 430 parking spots using a test vehicle equipped with four surround-view fisheye cameras, four wheel encoders, and an IMU, all synchronized and calibrated offline. The four fisheye cameras formed an AVM subsystem for real-time bird’s eye view stitching at 30Hz.

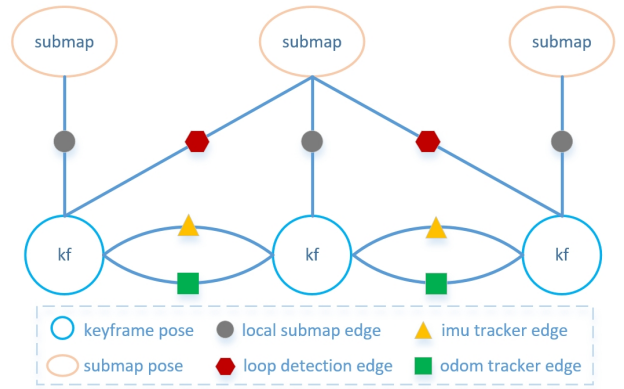


Fig. 6: Schematically of pose-graph with additional kinematic constraints

The proposed benchmark dataset to be publicly included four fisheye image sequences, one BEV image sequence, four wheel encoder data, and one IMU data. Fisheye images had a resolution of 1280×960, and BEV images had a resolution of 1354×1632, representing a physical area of 14.25m×17.18m (1.05cm per pixel on the ground). Both image sequences were stored at 10Hz. Our system used the BEV image as input for validation, while other visual algorithms used front fisheye camera images, which did not affect their operation.

B. Robustness and Accuracy of Mapping

It is well known that underground garages do not have the GPS signals to construct ground truth by using GPS-based Real-time Kinematic (RTK), and their repetitive structures and variable environments do not allow the use of structure-based lidar to construct ground truth. Therefore, we designed the following method to verify the robustness and accuracy of the proposed method.

- Robustness

We used images from a front-mounted fisheye camera as input and tried to run feature-based ORB-SLAM3 [3], optical flow based SVO [4] and DSO [5], and vision-inertia fusion based VINS-Mono [9]. Unexpectedly the traditional visual SLAM for the above state-of-the-art (SOTA) all suffer from initialization failures, frequent loss of tracking, and runtime failure because of the poor lighting, sparse texture, and scene variability of garage. On the other hand, the method in this paper is very stable because it adopts the vision-inertia-wheel fusion method for pose tracking and uses the semantic features of the road marking extracted from the bird’s-eye view to construct the map. The tracking and mapping are stable using datasets under different conditions, which confirms the robustness and reliability of our algorithm.

- Accuracy

Firstly, a comparative experiment was conducted based on the benchmark dataset 1. The map constructed from the poses output by the VIWFusion module is shown in Fig. 7. It is clear that there is an unavoidable accumulated error in the front-end. The back-end of Mapping is used with loop detection and global optimization techniques, which effectively eliminates the long-term drift and improves the

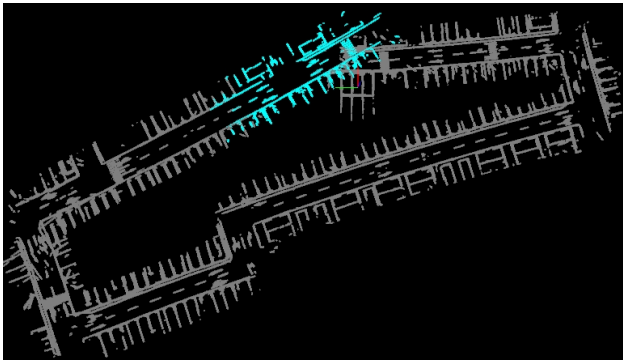
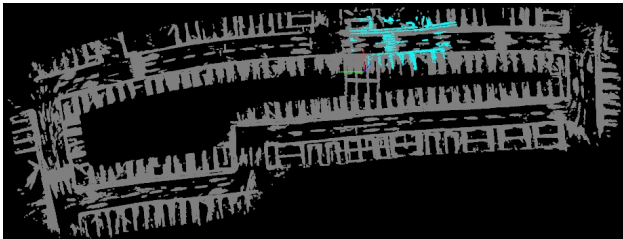
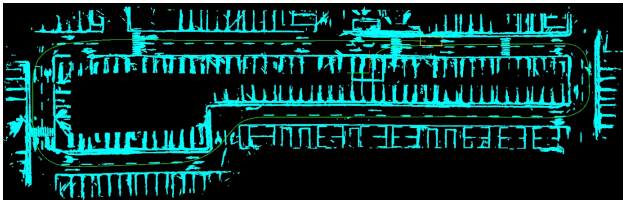


Fig. 7: Semantic map constructed from the poses of the VIWFusion module



(a) regular loop detection without extra kinematic constraints



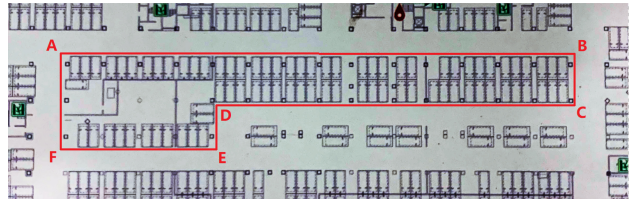
(b) SPQ loop detection with extra kinematic constraints

Fig. 8: Results of pose-graph optimization

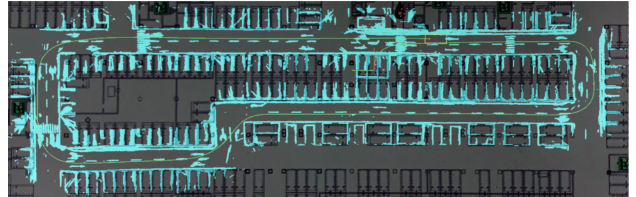
accuracy of mapping. Fig. 8a shows the results of pose-graph optimization via regular loop detection without extra kinematic constraints. Fig. 8b shows the results of pose-graph optimization via SPQ loop detection with extra kinematic constraints. It can be seen that the pose-graph optimization with the results of SPQ loop detection and extra kinematic constraints can construct more realistic maps.

Secondly, we performed a qualitative analysis using a schematic map of the planar structure of the garage (as shown in Fig. 9a) with the semantic map we constructed. The two are made to have the same size by scaling and are overlapped for comparison, as shown in Fig. 9b. Obviously, the semantic map built by our system can be perfectly aligned with the schematic map of the garage, with very high mapping accuracy.

Finally, we conducted a quantitative analysis by comparing the world distances between the six points, denoted as ABCDEF in Fig.9a, with the corresponding map distances. The world distances were measured using a high-precision laser rangefinder, while the map distances were computed from the respective 3D point coordinates. Table I presents the mean values of multiple measurements for both world distances and map distances. Table II shows the mean



(a) schematic map of garage



(b) overlapping comparison

Fig. 9: Qualitatively results of overlapping comparison

absolute error, maximum error, and root mean square error (RMSE) between these map distances and world distances, and attaches experimental data from the AVP-SLAM [22] and BEV Edge SLAM [24] for comparison. It should be noted that the authors of these two methods have not open-sourced them, so the data in the table are derived from the literature. Although the datasets are different, the application scenarios of the three methods are all underground garage, so they can still be used as references to each other. From Table II, it is obvious that ours AVM-SLAM system fusing multi-sensors has a higher accuracy of mapping.

TABLE I: Measurement of world distances and map distances

Meas.	AB[m]	BC[m]	CD[m]	DE[m]	EF[m]	FA[m]
Word	118.366	12.219	83.720	11.340	35.345	22.100
Map	117.896	11.792	82.307	10.314	35.258	22.585

TABLE II: Absolute Error of mapping

Method	Mean [m]	Max [m]	RMSE [m]
AVP-SLAM	/	8.32	4.31
BEV Edge SLAM	1.225	1.918	1.310
AVM-SLAM	0.651	1.413	0.785

VI. CONCLUSIONS

In this paper, we propose an AVM-SLAM framework for AVP tasks, equipped with four surround fisheye cameras, four wheel encoders, and an IMU. The system generates a BEV image using the AVM subsystem, and a convolutional neural network extracts garage road markings for mapping and localization. We employ a loosely weighted fusion front-end and a tightly-coupled back-end optimization to enhance robustness and accuracy by fusing wheel encoder and IMU data. Additionally, we provide a large-scale high-resolution benchmark dataset for garage localization and mapping development and evaluation. Experimental results validate our approach for AVP tasks in garages. Future work includes refining AVM-SLAM, optimizing multi-sensor fusion, and improving flare removal and semantic segmentation models.

REFERENCES

- [1] R. Mur-Artal, J. M. M. Montiel, and J. D. Tardós, “Orb-slam: a versatile and accurate monocular slam system,” *IEEE transactions on robotics*, vol. 31, no. 5, pp. 1147–1163, 2015.
- [2] R. Mur-Artal and J. D. Tardós, “Orb-slam2: An open-source slam system for monocular, stereo, and rgb-d cameras,” *IEEE transactions on robotics*, vol. 33, no. 5, pp. 1255–1262, 2017.
- [3] C. Campos, R. Elvira, J. J. G. Rodríguez, J. M. Montiel, and J. D. Tardós, “Orb-slam3: An accurate open-source library for visual, visual-inertial, and multimap slam,” *IEEE Transactions on Robotics*, vol. 37, no. 6, pp. 1874–1890, 2021.
- [4] C. Forster, M. Pizzoli, and D. Scaramuzza, “Svo: Fast semi-direct monocular visual odometry,” in *2014 IEEE international conference on robotics and automation (ICRA)*, pp. 15–22, IEEE, 2014.
- [5] J. Engel, V. Koltun, and D. Cremers, “Direct sparse odometry,” *IEEE transactions on pattern analysis and machine intelligence*, vol. 40, no. 3, pp. 611–625, 2017.
- [6] W. Hess, D. Kohler, H. Rapp, and D. Andor, “Real-time loop closure in 2d lidar slam,” in *2016 IEEE international conference on robotics and automation (ICRA)*, pp. 1271–1278, IEEE, 2016.
- [7] J. Zhang and S. Singh, “Loam: Lidar odometry and mapping in real-time,” in *Robotics: Science and systems*, vol. 2, pp. 1–9, Berkeley, CA, 2014.
- [8] T. Shan and B. Englot, “Lego-loam: Lightweight and ground-optimized lidar odometry and mapping on variable terrain,” in *2018 IEEE/RSJ International Conference on Intelligent Robots and Systems (IROS)*, pp. 4758–4765, IEEE, 2018.
- [9] T. Qin, P. Li, and S. Shen, “Vins-mono: A robust and versatile monocular visual-inertial state estimator,” *IEEE Transactions on Robotics*, vol. 34, no. 4, pp. 1004–1020, 2018.
- [10] T. Qin, J. Pan, S. Cao, and S. Shen, “A general optimization-based framework for local odometry estimation with multiple sensors,” *arXiv preprint arXiv:1901.03638*, 2019.
- [11] P. Geneva, K. Eickenhoff, W. Lee, Y. Yang, and G. Huang, “Openvins: A research platform for visual-inertial estimation,” in *2020 IEEE International Conference on Robotics and Automation (ICRA)*, pp. 4666–4672, IEEE, 2020.
- [12] X. Zuo, Y. Yang, P. Geneva, J. Lv, Y. Liu, G. Huang, and M. Pollefeys, “Lic-fusion 2.0: Lidar-inertial-camera odometry with sliding-window plane-feature tracking,” in *2020 IEEE/RSJ International Conference on Intelligent Robots and Systems (IROS)*, pp. 5112–5119, IEEE, 2020.
- [13] W. Shao, S. Vijayarangan, C. Li, and G. Kantor, “Stereo visual inertial lidar simultaneous localization and mapping,” in *2019 IEEE/RSJ International Conference on Intelligent Robots and Systems (IROS)*, pp. 370–377, IEEE, 2019.
- [14] K. J. Wu, C. X. Guo, G. Georgiou, and S. I. Roumeliotis, “Vins on wheels,” in *2017 IEEE International Conference on Robotics and Automation (ICRA)*, pp. 5155–5162, IEEE, 2017.
- [15] J. Liu, W. Gao, and Z. Hu, “Visual-inertial odometry tightly coupled with wheel encoder adopting robust initialization and online extrinsic calibration,” in *2019 IEEE/RSJ International Conference on Intelligent Robots and Systems (IROS)*, pp. 5391–5397, IEEE, 2019.
- [16] W. Lee, K. Eickenhoff, Y. Yang, P. Geneva, and G. Huang, “Visual-inertial-wheel odometry with online calibration,” in *2020 IEEE/RSJ International Conference on Intelligent Robots and Systems (IROS)*, pp. 4559–4566, IEEE, 2020.
- [17] Y. Niu, J. Liu, X. Wang, W. Hao, W. Li, and L. Chen, “Accurate and robust odometry by fusing monocular visual, inertial, and wheel encoder,” *CCF Transactions on Pervasive Computing and Interaction*, vol. 2, pp. 275–287, 2020.
- [18] H. Grimmert, M. Buerki, L. Paz, P. Pinies, P. Furgale, I. Posner, and P. Newman, “Integrating metric and semantic maps for vision-only automated parking,” in *2015 IEEE International Conference on Robotics and Automation (ICRA)*, pp. 2159–2166, IEEE, 2015.
- [19] U. Schwesinger, M. Bürki, J. Timpner, S. Rottmann, L. Wolf, L. M. Paz, H. Grimmert, I. Posner, P. Newman, C. Häne, *et al.*, “Automated valet parking and charging for e-mobility,” in *2016 IEEE Intelligent Vehicles Symposium (IV)*, pp. 157–164, IEEE, 2016.
- [20] Z. Xiang, J. Yu, J. Li, and J. Su, “Vilivo: Virtual lidar-visual odometry for an autonomous vehicle with a multi-camera system,” in *2019 IEEE/RSJ International Conference on Intelligent Robots and Systems (IROS)*, pp. 2486–2492, IEEE, 2019.
- [21] J. Hu, M. Yang, H. Xu, Y. He, and C. Wang, “Mapping and localization using semantic road marking with centimeter-level accuracy in indoor parking lots,” in *2019 IEEE Intelligent Transportation Systems Conference (ITSC)*, pp. 4068–4073, IEEE, 2019.
- [22] T. Qin, T. Chen, Y. Chen, and Q. Su, “Avp-slam: Semantic visual mapping and localization for autonomous vehicles in the parking lot,” in *2020 IEEE/RSJ International Conference on Intelligent Robots and Systems (IROS)*, pp. 5939–5945, IEEE, 2020.
- [23] X. Shao, L. Zhang, T. Zhang, Y. Shen, H. Li, and Y. Zhou, “A tightly-coupled semantic slam system with visual, inertial and surround-view sensors for autonomous indoor parking,” in *Proceedings of the 28th ACM International Conference on Multimedia*, pp. 2691–2699, 2020.
- [24] Z. Xiang, A. Bao, and J. Su, “Hybrid bird’s-eye edge based semantic visual slam for automated valet parking,” in *2021 IEEE International Conference on Robotics and Automation (ICRA)*, pp. 11546–11552, IEEE, 2021.
- [25] C. Zhang, H. Liu, Z. Xie, K. Yang, K. Guo, R. Cai, and Z. Li, “Avp-loc: Surround view localization and relocalization based on hd vector map for automated valet parking,” in *2021 IEEE/RSJ International Conference on Intelligent Robots and Systems (IROS)*, pp. 5552–5559, IEEE, 2021.
- [26] J. Kannala and S. S. Brandt, “A generic camera model and calibration method for conventional, wide-angle, and fish-eye lenses,” *IEEE transactions on pattern analysis and machine intelligence*, vol. 28, no. 8, pp. 1335–1340, 2006.
- [27] O. Ronneberger, P. Fischer, and T. Brox, “U-net: Convolutional networks for biomedical image segmentation,” in *Medical Image Computing and Computer-Assisted Intervention—MICCAI 2015: 18th International Conference, Munich, Germany, October 5–9, 2015, Proceedings, Part III 18*, pp. 234–241, Springer, 2015.
- [28] J. Johnson, A. Alahi, and L. Fei-Fei, “Perceptual losses for real-time style transfer and super-resolution,” in *Computer Vision—ECCV 2016: 14th European Conference, Amsterdam, The Netherlands, October 11–14, 2016, Proceedings, Part II 14*, pp. 694–711, Springer, 2016.
- [29] R. Li, J. Pan, Y. Si, B. Yan, Y. Hu, and H. Qin, “Specular reflections removal for endoscopic image sequences with adaptive-rpca decomposition,” *IEEE transactions on medical imaging*, vol. 39, no. 2, pp. 328–340, 2019.
- [30] R. Suvorov, E. Logacheva, A. Mashikhin, A. Remizova, A. Ashukha, A. Silvestrov, N. Kong, H. Goka, K. Park, and V. Lempitsky, “Resolution-robust large mask inpainting with fourier convolutions,” in *Proceedings of the IEEE/CVF winter conference on applications of computer vision*, pp. 2149–2159, 2022.
- [31] H. Zhao, J. Shi, X. Qi, X. Wang, and J. Jia, “Pyramid scene parsing network,” in *Proceedings of the IEEE conference on computer vision and pattern recognition*, pp. 2881–2890, 2017.
- [32] L.-C. Chen, Y. Zhu, G. Papandreou, F. Schroff, and H. Adam, “Encoder-decoder with atrous separable convolution for semantic image segmentation,” in *Proceedings of the European conference on computer vision (ECCV)*, pp. 801–818, 2018.
- [33] K. Sun, B. Xiao, D. Liu, and J. Wang, “Deep high-resolution representation learning for human pose estimation,” in *Proceedings of the IEEE/CVF conference on computer vision and pattern recognition*, pp. 5693–5703, 2019.
- [34] Y. Hong, H. Pan, W. Sun, and Y. Jia, “Deep dual-resolution networks for real-time and accurate semantic segmentation of road scenes,” *arXiv preprint arXiv:2101.06085*, 2021.